A New Microfluidics-Based Droplet Dispenser for ICPMS

Pascal E. Verboket,[†,§] Olga Borovinskaya,[‡,§] Nicole Meyer,[‡] Detlef Günther,*[‡] and Petra S. Dittrich*[†]

[†]Laboratory of Organic Chemistry, and [‡]Laboratory of Inorganic Chemistry, Department of Chemistry and Applied Biosciences, ETH Zurich, 8093 Zurich Switzerland

S *Supporting Information*

ABSTRACT: In this work, a novel droplet microfluidic sample introduction system for inductively coupled plasma mass spectrometry (ICPMS) is proposed and characterized. The cheap and disposable microfluidic chip generates droplets of an aqueous sample in a stream of perfluorohexane (PFH), which is also used to eject them as a liquid jet. The aqueous droplets remain intact during the ejection and can be transported into the ICP with >50% efficiency. The transport is realized via a custom-built system, which includes a membrane desolvator necessary for the PFH vapor removal. The introduction system presented here can generate highly monodisperse droplets in the size range of 40−60 μm at frequencies from 90 to 300 Hz. These droplets produced very stable signals with a relative standard deviation (RSD) comparable to the one achieved with a commercial droplet dispenser. Using the current system, samples with a total volume of <1 μL can be analyzed. Moreover, the capabilities of the setup for introduction and quantitative elemental analysis of single cells were described using a test system of bovine red blood cells. In the future, other modules of the modern microfludics can be integrated in the chip, such as on-chip sample pretreatment or parallel introduction of different samples.
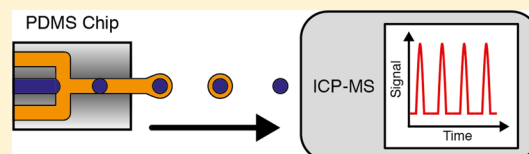
Conventionally, elemental analysis of liquids in the inductively coupled plasma optical emission spectrometry (ICP-OES) and inductively coupled plasma mass spectrometry (ICPMS) is realized by means of pneumatic nebulizers in combination with spray chambers.[1] The operating principle of such a sample introduction system is based on the conversion of a liquid into a polydisperse aerosol (nebulizer) and subsequent filtering out of large droplets (spray chamber). These systems exist in various geometries, are robust, and are routinely used in many applications.[2] Their main drawback, however, is a high sample consumption (designed to run with the liquid flow of >0.3 mL min^{-1})[3] and an incomplete sample transport, which limit their applicability for the analysis of micro sample volumes commonly available in biological, forensic, toxicological, and clinical studies.[4] Reducing the nebulizer nozzle dimensions has decreased the effective sample consumption from a few milliliters per minute to microliters per minute and even nanoliters per minute[5] and has significantly enhanced the aerosol transport efficiency (TE) thanks to a much lower sample uptake.[4] These days, there are many variations of microflow nebulizers, which can operate with close to 70−100% sample TE with or without spray chambers[6,7] and desolvation systems; these include the microconcentric nebulizer,[8] micromist nebulizer,[8] high-efficiency nebulizer,[9] and direct injection high-efficiency nebulizer.[10] Reduction of the nebulizer opening dimensions, however, leads directly to the increased risk of clogging whenever samples containing highly concentrated salts or undigested biological fluids have to be analyzed.[4] In addition, the highest stability of the aerosol production in microflow nebulizers is achieved by passive liquid uptake,[11] whose rate depends on the pressure difference at both ends of the

nebulizer capillary that is directly determined by the nebulizing gas flow rate. Since the range of the optimum flow rate of this gas is normally very narrow, the flexibility of the system in terms of the sample uptake is also limited.

A new concept of injecting the liquid sample into the ICP in the form of monodisperse discrete droplets was introduced by Olesik and Hobbs.[12] Uniform ≈50 μm droplets could be produced on demand by a micropump,[13] which ejected a defined liquid volume after capillary contraction, and transported via a laminar flow oven into the ICP with 100% efficiency. This system did not find wide application but has significantly contributed to the fundamental understanding of analyte behavior in analytical ICPs.[14]

A system for controlled generation of monodisperse microdroplets consisting of a piezoelectrically driven dispenser head, a control box, and a droplet visualization system is commercially available (Microdrop Technologies GmbH, Norderstedt, Germany). The droplets can be produced in sizes of 30, 50, 70, and 100 μm in a frequency range from 100 Hz to a few kilohertz with only 1% droplet variation in volume, and liquid volume flow rates of picoliters per minute to nanoliters per minute can be measured. The transport of these relatively large droplets into the ICPMS was realized using ambient temperature desolvation with helium[15] instead of argon[16] as a carrier gas.[17,18] The droplets can be transported into the plasma either vertically or horizontally, depending on their size, with close to 100% efficiency.[19] This system has already shown its potential in quantitative analysis of single

nanoparticles[19,20] and characterization of individual biological cells by ICPMS,[21] which has recently gained great interest in the field of nanosafety[22] and in cell biology.[23] Another similar system based on the thermal inkjet technology has been recently introduced[24] and successfully applied to the elemental analysis of urine using dosing frequency calibration.[25]

Even though the single-droplet introduction is very efficient and promising for the analysis of micro sample volumes or single entities such as nanoparticles and cells, the currently available microdispenser modules have several drawbacks. They provide droplets with a fixed volume, which is set by the nozzle diameter and can only slightly be varied by dispenser settings (unless custom settings are used[17]), are sensitive to the changes of the physical properties of the liquid (salt content, pH), are prone to clogging, difficult to clean, and rather expensive. In addition, efficient and nondestructive introduction of cells might be problematic due to the passive liquid uptake through the capillary and the application of a high voltage.

In this work a different approach to generate microdroplets for ICPMS analysis using droplet microfluidics is presented. Droplet microfluidics has been intensively used for studying (bio)chemical reactions[26−29] and for single-cell studies.[30,31] Recently, it has been proposed as a valuable system for sample preparation in matrix-assisted laser desorption/ionization mass spectrometry[32] and as sample introduction system for electrospray mass spectrometry.[33,34] In our interface, monodisperse aqueous droplets are produced using the highly volatile carrier phase perfluorohexane (PFH) in a custom-designed liquid-assisted droplet ejection (LADE) chip, which is made entirely of poly(dimethylsiloxane) (PDMS). The chip is cheap, disposable, can produce droplets in a broader volume range and is more robust to changes of liquid sample properties. Interfacing of the new chip with the ICPMS was accomplished via a custom-built transport system including a membrane desolvator, which permitted the PFH vapor removal. This paper summarizes characterization and optimization of the system and its application for the analysis of single bovine blood cells.

■ EXPERIMENTAL SECTION

Materials. SU-8 2002 and SU-8 2050 photoresists were purchased from Microchem Corp. (Massachusetts, U.S.A.). $1H,1H,2H,2H$-Perfluorodecyltrichlorosilane was purchased from ABCR-Chemicals (Karlsruhe, Germany). PDMS and curing agent (Sylgard 184) were obtained from Dow Corning (Michigan, U.S.A.). Perfluorohexane, 95+% and 99% (used for the ICPMS tests), were purchased from Alfa Aesar (Karlsruhe, Germany) and Sigma-Aldrich (Missouri, U.S.A.), respectively. Merck IV multielement standard solution was purchased from Merck Millipore (Massachusetts, U.S.A.). The test solutions were prepared from single-element standard solutions (Inorganic Ventures, Virginia, U.S.A.) and contained nitrate salts of either Ce or Na, Mg, Ca, Mn, Fe, Mo (referred as multielement solution) at concentrations of 1 mg kg^{-1}. Merck IV and the test solutions were diluted to the required concentrations with 2% sub-boiled HNO_3 prepared in ultrahigh-purity water (Merck Millipore, Massachusetts, U.S.A.).

Cell Preparation and Digestion. Washed pooled bovine/calf red blood cells in phosphate-buffered saline (PBS) were obtained from Rockland Immunochemicals Inc. (Pennsylvania, U.S.A.). Additional PBS for dilution of the cell suspension was purchased from Life Technologies (Paisley, U.K.). The concentration of cells was manually determined using a hemocytometer (five replicates). Three aliquots of 1 mL of the cell suspension were microwave digested (Ethos Plus, Milestone Inc., Connecticut, U.S.A.) in 8 mL of 60% sub-boiled HNO_3 and 2 mL of 30% H_2O_2 (TraceSelect, Fluka Analytical, Buchs SG, Switzerland) adding Co to determine the digestion recovery. After 5000× dilution of the dissolved cell suspension, the quantification of Fe was realized by ICPMS using external calibration and Mn as internal standard. Acid and PBS blanks were monitored in the same way.

Microfluidic Chip Fabrication. The microfluidic chip consists of two PDMS pieces that are bonded together. One half is patterned with the microfluidic channels and the other half is flat and used to seal the channels. The PDMS was prepared by mixing the oligomer and the curing agent at a ratio of 10:1. After degassing the PDMS mixture it was poured into a custom-made casting form placed on top of a silicon wafer. All details of the master mold fabrication can be found in the Supporting Information. The casting form has an opening allowing filling with PDMS and provides the semicircular shape. The chips for use on the microscope were fabricated in a rectangular shape with an open-top casting form. The PDMS was cured at 150 °C for 6 min. Holes were punched in the patterned PDMS half using a 1.5 mm outer diameter biopsy puncher (Miltex, Pennsylvania, U.S.A.) to form the inlets. The layers were then bonded together by adhesive bonding using the PDMS curing agent.[35] A blank 100 mm carrier wafer was spin-coated with PDMS curing agent for 30 s at 6000 rpm. Subsequently, the patterned PDMS half was stamped onto the coated carrier wafer and then manually aligned on top of the flat PDMS half. After curing for 24 h at room temperature the tip of the chip was cut off with a utility knife opening the outlet nozzle. It has a rectangular shape with the dimensions of approximately 40 μm × 25 μm (Supporting Information Figure S-1). Finally, the microfluidic channels were silanized by flushing for 20 min with a stream of dry N_2 carrying $1H,1H,2H,2H$-perfluorodecyltrichlorosilane to achieve a more robust droplet generation. All steps of the chip fabrication are shown in detail on the Figures S-2 and S-3 in the Supporting Information. The entire chip design including all feed lines is shown in Supporting Information Figure S-4.

Microfluidic Chip Operation. All fluids were supplied using a neMESYS syringe pump (Cetoni, Korbussen, Germany). The aqueous sample solutions were added with a 1 mL Primo syringe (Codan, Lensahn, Germany), at flow rates of 0.3−1 μL min^{-1}. PFH for generation and acceleration of droplets was delivered at flow rates between 30 and 100 μL min^{-1} with 5 mL syringes (B. Braun, Melsungen, Germany). Fluids from the syringes were transferred to the LADE chip using PTFE tubing (PKM SA, Lyss, Switzerland). After the flows were started, 3−5 min was required to fill the microfluidic channels with liquid and to stabilize the droplet generation.

Optical Droplet Measurements. Bright-field microscopy was performed on an Olympus IX71 inverted microscope (Tokyo, Japan) with a Miro M110 high-speed camera (Vision Research, New Jersey, U.S.A.). The LADE chips for microscopic use were mounted horizontally on a custom-made microscope insert. This insert holds the chip in place above a plastic Petri dish, which collected the ejected liquids. The high-speed recordings were analyzed using the droplet morphometry and velocimetry software[36] to obtain droplet size and droplet frequency statistics. All images were recorded at 10 000 frames s^{-1} with an exposure time of 10 μs. Before each measurement

the system was given at least 3 min to stabilize. The droplet size and frequency for various flow rates of deionized H_2O and PFH were measured twice for 1 s on two different chips (in total four measurements). The average of the frequency and droplet size of these four measurements was calculated. The experiments with deionized H_2O, Merck IV solution, and PBS were performed on three different chips. Each solution was measured once for 1 s, and the average droplet size and frequency were calculated.

Droplet Transport System. The setup of the droplet transport system is shown in Figure 1. The droplet jet was
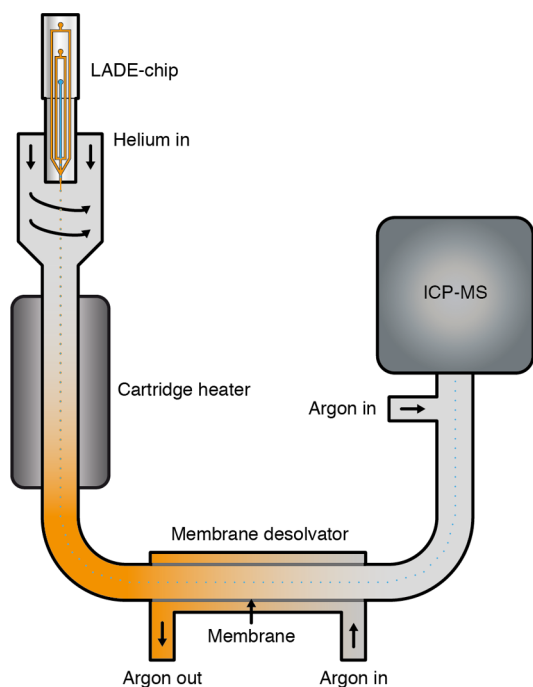

Figure 1. Schematic drawing of the experimental setup (not to scale). The system consists of the LADE chip, a heater, a membrane desolvator, and an ICPMS.

ejected vertically into a custom-built adapter made of poly(methyl methacrylate) (PMMA). A cyclonic gas flow of He supplied through the adapter transported the droplets further into a vertically arranged stainless steel tube with 6 mm inner diameter and 50 cm length. A cartridge heater placed in the middle of the steel tube was used to accelerate the solvent evaporation and to reduce the total droplet size permitting its further transport. A poly(vinyl chloride) (PVC) tubing was used to connect the steel tube with a membrane desolvator (CETAC6000AT$^+$ (only the desolvator unit), CETAC Technologies, Nebraska, U.S.A.), whose operating parameters are summarized in Table 1. The dry droplets were introduced into the ICP after admixing with Ar via a laminar flow adapter

Table 1. Optimized Operating Parameters of the Transport System and ICPMS

cartridge heater	30 W
He gas flow rate	0.6−0.8 L min^{-1}
desolvator membrane temperature	160 °C
desolvator sweep gas flow rate	3−4 L min^{-1}
Ar gas flow rate	0.1 L min^{-1}
ICP plasma power	1300 W

to maintain stable operating conditions within the ICP. Besides the microfluidic chip, a commercially available microdroplet dispensing system consisting of a dispenser head, a control unit, and a CCD camera for the droplet visualization (MD-K-150 with control unit MD-E-201-H, Microdrop Technologies GmbH, Norderstedt, Germany) was used with the same transport setup for comparison experiments.

ICPMS. A commercial quadrupole-based ICPMS (ELAN6000, PerkinElmer, Massachusetts, U.S.A.) was employed in this work. Its operating conditions are summarized in Table 1. The data was read out every 10 ms with 3 ms interval in between, resulting in the measurement duty cycle of 77%.

Data Evaluation. The MS-signals generated by droplets were evaluated using OriginPro 8.6 (OriginLab Corp., Massachusetts, U.S.A.). The signals were plotted as frequency distribution histograms, which were subsequently fitted with the Gaussian function. The mean and σ of the fit represented the mean signal intensity and its standard deviation (SD), respectively. The transport efficiency was derived from the total number of droplet events detected per total effective measurement time (only the dwell time) and the droplet production frequency. The total number of droplets was estimated summing up all the transient signals. The intervals for signals produced by one, two, and more droplets were chosen based on minima of their frequency distribution histogram.

■ RESULTS AND DISCUSSION

Microfluidic Device. A photograph of the LADE chip is shown in Figure 2a. It is made entirely of PDMS by means of
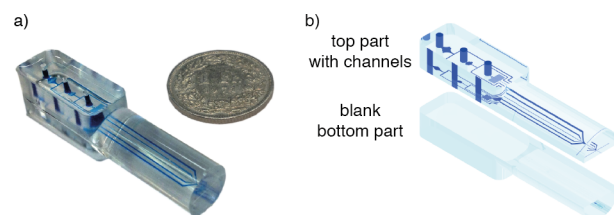

Figure 2. (a) Photograph of the LADE chip next to a one Swiss franc coin for scale. All fluidic channels are filled with blue food dye for visualization. The round part of the chip can be directly inserted into a socket of the adapter. The rectangular part of the chip contains the three access holes for sample and PFH introduction. (b) Rendering of the two components of the LADE chip.

standard soft lithography. One part of the chip was designed to be cylindrical so that it fits tightly into the inlet of the droplet transport system. To achieve this round shape a custom-made casting form was produced. The chip is composed of two halves (Figure 2b). Due to the low cost of the material (approximately $2 per chip) and the fast fabrication time (about 15 min hands on time per chip, excluding the wafer fabrication) the use of a new chip for every experiment is feasible, which eliminates cross contamination and the need for time-consuming cleaning. Furthermore, the fabrication technique allows for fast changes of the design and the integration of additional microfluidic components.

Figure 3a shows a scheme of the key microfluidic features of the LADE chip. In the first channel junction, monodisperse droplets of an aqueous sample solution are generated. The aqueous phase is segmented by flow focusing using the immiscible and highly volatile PFH (boiling point 58−60 °C).[37] Size and frequency of the droplets can be controlled by
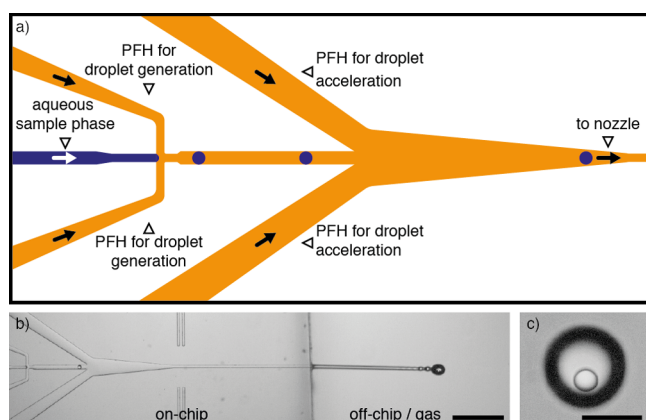
Figure 3. (a) Scheme of droplet generation and acceleration. In the first junction monodisperse aqueous droplets are generated in the stream of PFH. To accelerate the droplets, further PFH is added at the second junction. Subsequently, the droplet stream exits the LADE chip through the nozzle. Arrows indicate the direction of the flows for liquid streams. (b) Micrograph showing the on-chip droplet generation and acceleration as well as the ejection from the chip. Scale bar 500 μm. (c) Micrograph of an aqueous droplet and its surrounding PFH after ejection from the LADE chip. Scale bar 100 μm.

the flow rates of the aqueous phase and the PFH. The second junction is used to add more PFH in order to increase the flow speed to at least 1 m s^{-1}, which is necessary for the ejection of the liquid in a stable and straight jet (Figure 3b and the Supporting Information movie). This double-junction design allows controlling the jet stability independent from droplet generation, enabling the production of a broader range of droplet sizes. Furthermore, this concept simplifies the integration of further microfluidic components. It is also an advantage that the liquid sample droplets do not get into direct contact with the nozzle, which prevents clogging of the nozzle by dried residues. After ejection, the PFH carrier phase breaks into small droplets, whereas the aqueous droplets remain intact inside a PFH shell (Figure 3c). Fragmentation of the aqueous droplets during the ejection was not observed under the microscope.

System Characterization. The droplet sizes and frequencies were characterized with a high-speed camera and an automated image-processing program. The results (shown in Table 2) from the two chips demonstrate the droplet monodispersity and a low chip-to-chip variation. The size of the on-chip produced aqueous droplets ranges from 40 to 60

μm in diameter (30−110 pL). However, the droplet size range can easily be extended by changing the channel height or chip design. The influence of the dissolved substance in the aqueous phase on the droplet generation was insignificant (see Table 3). This indicates that the system can potentially be used for various aqueous solutions without the need for an individual measurement of the frequency and size.

A transient MS-signal generated by one single droplet is very short and lasts only a few hundreds of microseconds.[38] These signals could not be temporally resolved with the MS used (10 ms dwell time). The transient signals of single droplets containing Ce nitrate solution and their frequency distribution histogram are shown in Figure 4, parts a and b. The double distribution (not including the first tailing peak) is the result of a high temporal jitter in droplet arrival at the ICP (>10 ms) and unsynchronized signal acquisition. It corresponds to the signal of one (630 ± 50) or two (1250 ± 70) droplets detected within the dwell time of 10 ms. Table 4 summarizes the relative standard deviation (RSD) of signals of single droplets for several other isotopes measured using a multielement solution at a concentration of 1 mg kg^{-1}.

The signal precision is not only a function of the variation in droplet volume but also of the multiplicative noise related to the transport system and the ICP and of the Poisson noise.[39] An additional source leading to a broadening of the signal distribution is the incomplete signal detection due to splitting of single-droplet signals between the dwell time (10 ms) and quadrupole settling time (3 ms). This can be eliminated employing continuous, time-resolved detection.[15,40] A signal RSD as low as 8% was achieved, which is comparable to the RSDs obtained using the commercially available microdroplet generator system and indicates high monodispersity of the aqueous droplets generated by the chip.

The first peak of the intensity distribution histogram (Figure 4b from 0 to 25 counts/10 ms) cannot be attributed to the background only because of its longer tailing in comparison to the signal measured with the aqueous phase switched off, which amounted to only 2.8 ± 1.9 counts. The ratio of the mean of this peak to the mean of the next peak, which is produced by the single droplets, was element-specific and varied with operating conditions of the chip and the He gas flow rate. The appearance of the first peak can be mainly explained by disruption and fragmentation of the droplets during the transport and, additionally, by washout of a remaining on the channel walls aqueous solution by PFH plugs, or other memory effects within the transport system. Further studies are required to investigate this phenomenon in more detail.

Table 2. Droplet Size and Frequency for Various Flow Rates Measured Twice for 1 s on Two Separate Chips, with H$_2$O as Aqueous Phase

flow rate of H$_2$O [μL min^{-1}]	flow rate of PFH droplet generation [μL min^{-1}]	flow rate of PFH droplet acceleration [μL min^{-1}]	av droplet diameter [μm]	av droplet frequency [Hz]
0.3	35	35	57 ± 2	89.4 ± 3.8
0.3	40	40	54 ± 1	104.1 ± 16.7
0.3	50	50	47 ± 1	158.8 ± 22.6
0.3	60	60	44 ± 1	181.1 ± 24.1
0.5	35	35	57 ± 1	158.2 ± 10.1
0.5	35	40	58 ± 2	158.8 ± 31.0
0.5	35	50	57 ± 1	155.8 ± 5.6
0.5	40	40	55 ± 1	168.7 ± 17.6
0.5	50	50	49 ± 1	251.7 ± 36.8
0.5	60	60	43 ± 2	288.1 ± 24.7

Table 3. Droplet Size and Frequency for Three Different Solutions[a]

flow rate of aqueous sample [μL min^{-1}]	H$_2$O droplet frequency [Hz]	H$_2$O av droplet diameter [μm]	Merck IV droplet frequency [Hz]	Merck IV av droplet diameter [μm]	PBS droplet frequency [Hz]	PBS av droplet diameter [μm]
0.3	90.7	55 ± 2	90.1	57 ± 1	90.2	57 ± 1
0.5	145.5	56 ± 1	144.9	58 ± 1	146.7	58 ± 1

[a]The flow rate of PFH for droplet generation and acceleration was 35 μL min^{-1} each.
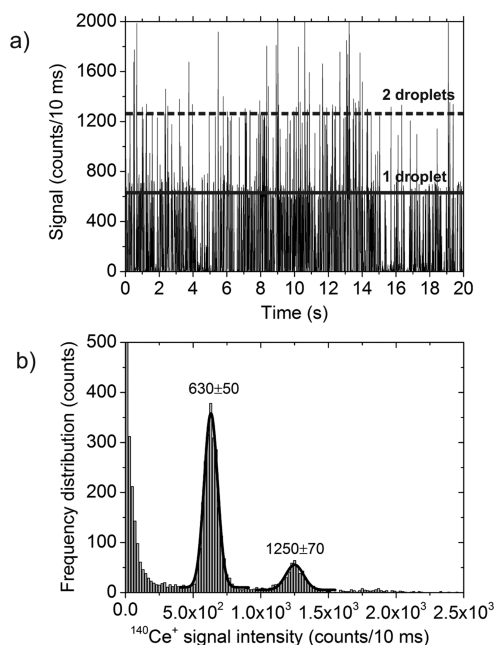

Figure 4. (a) Transient signals generated by droplets consisting of the Ce nitrate solution and (b) their frequency distribution histogram. The first and the second fitted peaks correspond to the signals of one and two droplets acquired within 10 ms dwell time, respectively. The Gaussian function was fitted to find the mean and SD of the signals. The droplets were produced using 0.3, 35, and 35 μL min^{-1} of aqueous solution, generating PFH, and accelerating PFH, respectively.

Table 4. RSDs of the Signals Generated from Single Droplets Consisting of the Multielement Solution[a]

isotope	RSD (%)
^{23}Na	11
^{55}Mn	8
^{56}Fe	11
^{95}Mo	13

[a]The droplets were produced using 0.5, 50, and 60 μL min^{-1} of aqueous solution, generating PFH, and accelerating PFH, respectively.

The TE of the droplets depended strongly on the He gas flow rate and reached its maximum at ≈65% (Supporting Information Figure S-5). The 58% maximum TE achieved using the commercial dispenser, which produced aqueous droplets in the size of 72.1 ± 0.5 μm at 10 Hz, suggests that the number of droplets delivered to the ICP is strictly limited by the transport assembly and not by the chip itself. The temporal jitter of droplets generated by the microdroplet dispenser was also significantly higher (>10 ms) than that reported using horizontal and vertical transport assemblies operated at ambient temperature.[19] Only a minor change in the droplet TE was observed varying the flow rate of the Ar sweep gas (Supporting Information Figure S-5). The current TE and high variation in arrival times of droplets at the plasma can be improved by

optimizing the geometry of the transport system, shortening the total distance between the position of droplet ejection and the ICP, and implementing the desolvation at a very early stage.

To increase the analysis throughput a discrete sampling strategy is of an advantage. Similar to the cartridge sampling technique,[41] small volumes of different samples can be introduced into a capillary between PFH plugs which will prevent their intermixing. A series of droplets of each sample plug produced on the chip can be sequentially measured. Approximately 0.5 μL of the multielement solution was measured in this way, and the signal of ^{56}Fe was monitored. The signal distribution histogram is shown in Figure 5. Even
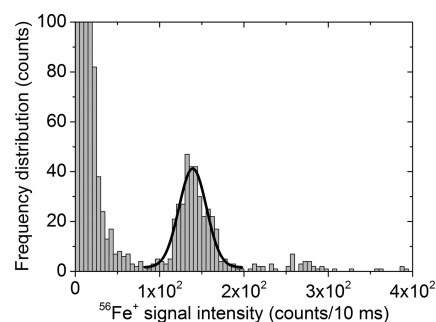

Figure 5. Frequency distribution histogram of signals generated by single droplets. Approximately 0.5 μL of the multielement solution was injected. The Gaussian function was fitted to find the mean and SD of the signals. The droplets were produced using flow rates of 0.5, 40, and 40 μL min^{-1} of aqueous solution, generating PFH, and accelerating PFH, respectively.

such a small liquid aliquot could still be measured and produced signals with an RSD of 11%. Approximately 8% of this RSD can be assigned to the contribution from counting statistics.[42]

Cell Analysis. The new system can be employed for introduction and subsequent analysis of single biological cells. First, tests were carried out using 6−7 μm in diameter bovine/calf red blood cells suspended in PBS. The suspension was diluted in PBS to a concentration of 1 × 10^7 cells/mL ensuring that only 7% of the droplets carry more than 1 cell. The sample was introduced at a rate of 0.5 μL min^{-1}, and the flow rates of the PFH generating and accelerating streams were 40 μL min^{-1}. Transient signals generated by single cells and their frequency distribution histogram are shown in Figure 6, parts a and b. A frequency distribution histogram of PBS signals without cells can be found in the Supporting Information (Figure S-6). The TE of the cells was significantly lower (4.5%) than the TE obtained with droplets containing multielement solution and degraded during the measurement due to the cell precipitation in the syringe and the capillary. No clogging of the microfluidic channels by cells after operation was detected under the optical microscope.

The size of the red blood cells is larger than the size of the completely desolvated salt particle, which would be ≈1 μm for
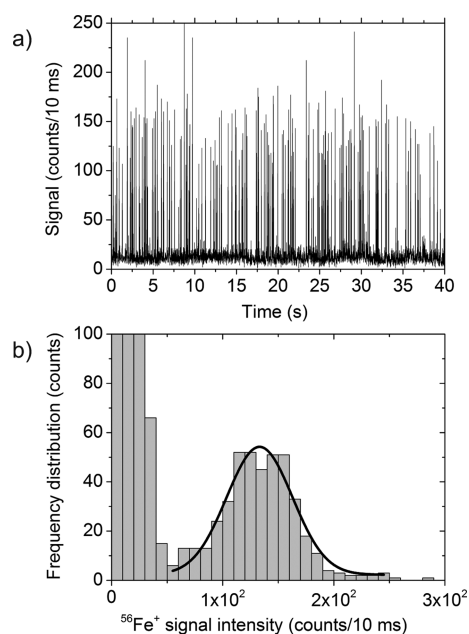
Figure 6. (a) $^{56}Fe^+$ transient signals generated by single red blood cells and (b) their frequency distribution histogram. The droplets were produced using flow rates of 0.5, 40, and 40 μL min^{-1} of aqueous solution, generating PFH, and accelerating PFH, respectively.

a 50 μm droplet generated from a 1 mg kg^{-1} multielement solution used in this work. Additionally, the high salt content of the PBS will result in an even larger residue of the droplet carrying the cell after liquid evaporation. Therefore, the low TE is most likely a result of losses in the transport assembly, whose length was relatively long and should be further optimized specifically for applications involving cells. Nevertheless, the RSD of the $^{56}Fe^+$ signals produced by single cells from the detected cell population amounted to 23% (Figure 6b).

The average number of Fe atoms/cell of $5.3 \pm 1.2 \times 10^8$ was determined based on calibration of the instrument with droplets consisting of the multielement solution. The cells and the standard solution were measured using two different chips. The mean signal intensity of the first background peak was subtracted from the mean signal generated by the single cells. The means were determined by fitting the distribution histograms with the Gaussian function. The first peak originates mostly from the ArO^+ polyatomic species interfering on the measured mass-to-charge ratio (m/Q); however, the contribution of Fe released from the cells to its tailing cannot be excluded. Employing the non-matrix-matched standard, the content of Fe per cell was underestimated by 25% compared to $6.2 \pm 0.6 \times 10^8$ atoms/cell calculated from the cell concentration and bulk concentration of Fe. This underestimation can be caused by incomplete vaporization of droplets residues carrying cells in the plasma[43] or by cell hemolysis.

It has already been demonstrated that the element content of individual cells can be quantitatively determined using calibration with solid particles[44] and monodisperse aerosols.[45] Recently, monodisperse microdroplets consisting of an inorganic salt standard solution were utilized for quantitative mass determination of single metallic nanoparticles.[19] This approach can be directly transferred to the quantification of naturally occurring or exogenous elements in single cells and quantification of the proteins after chemical and biospecific

labeling.[46] The recent developments in metal-based labeling of the cell proteome[47] and in the field of mass cytometry[48] have enabled multiplexing in the single-cell analysis and extended the use of the ICPMS to cell biology. The single-droplet-based calibration approach can expand the capabilities of the mass cytometry toward the absolute protein quantification in the cell, provided the labeling can be performed quantitatively. The results obtained with the microfluidic system demonstrate its potential toward quantitative metallomics and proteomics in bulk or on the single-cell basis. For a more accurate quantification, the system can be further modified in the way that the sample and standard can be introduced from the same chip in parallel or sequentially.

■ CONCLUSIONS

A novel droplet microfluidics-based sample introduction system for the ICPMS analysis of micro samples is described. The droplets generated in the microfluidic chip are highly monodisperse and can be produced in the size range from 40 to 60 μm. This size range, however, can be further extended by modifications of the microfluidic channels. The aqueous droplets ejected from the chip in the stream of PFH remain intact and can be transported into the ICPMS via a custom-built transport system with >50% efficiency. The ongoing work in our lab is currently focused on the improvement of this system to achieve complete and more stable sample transport. The proposed sample introduction system demonstrated its potential for the analysis of liquid volumes of <1 μL and for the quantitative elemental analysis of single cells. In this respect, the development of a chip capable of generating the droplets of sample and standard sequentially or in parallel[49] would be highly beneficial for the accurate quantification. In addition, the integration of a multichannel sample introduction can potentially be used for the internal standardization or to increase the measurement throughput by running more than one sample in parallel. This parallel approach will be valid only if isotope signatures of the samples are different. Furthermore, such an approach would require a simultaneous mass spectrometer. This new introduction technique has also a potential for the integration of further microfluidic modules for sample pretreatment, e.g., separation,[50−52] dilution,[53−55] fast mixing,[56] chemical reactions,[57] or cell sorting.[58,59] In addition, cells encapsulated inside the droplets can be lysed to reduce the volume of the cell residua and to possibly improve their transport efficiency.

■ ASSOCIATED CONTENT

ⓢ Supporting Information

Additional information as noted in text. This material is available free of charge via the Internet at http://pubs.acs.org.

■ AUTHOR INFORMATION

Corresponding Authors
*E-mail: guenter@inorg.chem.ethz.ch.
*E-mail: dittrich@org.chem.ethz.ch. Phone: 0041 44 633 68 93.

Author Contributions
§P.E.V. and O.B. contributed equally to this work.

Notes
The authors declare no competing financial interest.

REFERENCES

(1) Todoli, J.-L.; Mermet, J.-M. *Liquid Sample Introduction in ICP Spectrometry*; Elsevier: Amsterdam, The Netherlands, 2008.

(2) Montaser, A. *Inductively Coupled Plasma Mass Spectrometry*; Wiley-VCH: New York, 1998.

(3) Sutton, K. L.; B'Hymer, C.; Caruso, J. A. *J. Anal. At. Spectrom.* **1998**, *13*, 885−891.

(4) Todoli, J.-L.; Mermet, J.-M. *Spectrochim. Acta, Part B* **2006**, *61*, 239−283.

(5) Giusti, P.; Lobinski, R.; Szpunar, J.; Schaumlöffel, D. *Anal. Chem.* **2005**, *78*, 965−971.

(6) Todoli, J.-L.; Mermet, J.-M. *J. Anal. At. Spectrom.* **2002**, *17*, 345−351.

(7) Todoli, J.-L.; Mermet, J.-M. *Can. J. Anal. Sci. Spectrosc.* **2002**, *47*, 164−170.

(8) Todoli, J.-L.; Hernandis, V.; Canals, A.; Mermet, J.-M. *J. Anal. At. Spectrom.* **1999**, *14*, 1289−1295.

(9) Liu, H.; Montaser, A. *Anal. Chem.* **1994**, *66*, 3233−3242.

(10) McLean, J. A.; Zhang, H.; Montaser, A. *Anal. Chem.* **1998**, *70*, 1012−1020.

(11) Jensen, B. P.; Gammelgaard, B.; Hansen, S. H.; Andersen, J. V. *J. Anal. At. Spectrom.* **2003**, *18*, 891−896.

(12) Olesik, J. W.; Hobbs, S. E. *Anal. Chem.* **1994**, *66*, 3371−3378.

(13) French, J. B.; Etkin, B.; Jong, R. *Anal. Chem.* **1994**, *66*, 685−691.

(14) Olesik, J. W. *Appl. Spectrosc.* **1997**, *51*, A158−A175.

(15) Gschwind, S.; Flamigni, L.; Koch, J.; Borovinskaya, O.; Groh, S.; Niemax, K.; Günther, D. *J. Anal. At. Spectrom.* **2011**, *26*, 1166.

(16) Murtazin, A.; Groh, S.; Niemax, K. *J. Anal. At. Spectrom.* **2010**, *25*, 1395−1401.

(17) Shigeta, K.; Traub, H.; Panne, U.; Okino, A.; Rottmann, L.; Jakubowski, N. *J. Anal. At. Spectrom.* **2013**, *28*, 646−656.

(18) Franze, B.; Strenge, I.; Engelhard, C. *J. Anal. At. Spectrom.* **2012**, *27*, 1074−1083.

(19) Gschwind, S.; Hagendorfer, H.; Frick, D. A.; Günther, D. *Anal. Chem.* **2013**, *85*, 5875−5883.

(20) Garcia, C. C.; Murtazin, A.; Groh, S.; Horvatic, V.; Niemax, K. *J. Anal. At. Spectrom.* **2010**, *25*, 645−653.

(21) Shigeta, K.; Koellensperger, G.; Rampler, E.; Traub, H.; Rottmann, L.; Panne, U.; Okino, A.; Jakubowski, N. *J. Anal. At. Spectrom.* **2013**, *28*, 637−645.

(22) Laborda, F.; Bolea, E.; Jiménez-Lamana, J. *Anal. Chem.* **2014**, *86*, 2270−2278.

(23) Bendall, S. C.; Simonds, E. F.; Qiu, P.; Amir, E.-a. D.; Krutzik, P. O.; Finck, R.; Bruggner, R. V.; Melamed, R.; Trejo, A.; Ornatsky, O. I.; Balderas, R. S.; Plevritis, S. K.; Sachs, K.; Pe'er, D.; Tanner, S. D.; Nolan, G. P. *Science* **2011**, *332*, 687−696.

(24) Orlandini von Niessen, J. O.; Schaper, J. N.; Petersen, J. H.; Bings, N. H. *J. Anal. At. Spectrom.* **2011**, *26*, 1781−1789.

(25) Orlandini von Niessen, J. O.; Petersen, J. H.; Schaper, J. N.; Bings, N. H. *J. Anal. At. Spectrom.* **2012**, *27*, 1234−1244.

(26) Song, H.; Tice, J. D.; Ismagilov, R. F. *Angew. Chem., Int. Ed.* **2003**, *42*, 768−772.

(27) Dittrich, P. S.; Jahnz, M.; Schwille, P. *ChemBioChem* **2005**, *6*, 811−814.

(28) Li, L.; Mustafi, D.; Fu, Q.; Tereshko, V.; Chen, D. L.; Tice, J. D.; Ismagilov, R. F. *Proc. Natl. Acad. Sci. U.S.A.* **2006**, *103*, 19243−19248.

(29) Zhang, Q.; Liu, X.; Liu, D.; Gai, H. *Lab Chip* **2014**, *14*, 1395−1400.

(30) Baret, J. C.; Beck, Y.; Billas-Massobrio, I.; Moras, D.; Griffiths, A. D. *Chem. Biol.* **2010**, *17*, 528−536.

(31) Brouzes, E.; Medkova, M.; Savenelli, N.; Marran, D.; Twardowski, M.; Hutchison, J. B.; Rothberg, J. M.; Link, D. R.; Perrimon, N.; Samuels, M. L. *Proc. Natl. Acad. Sci. U.S.A.* **2009**, *106*, 14195−14200.

(32) Küster, S. K.; Fagerer, S. R.; Verboket, P. E.; Eyer, K.; Jefimovs, K.; Zenobi, R.; Dittrich, P. S. *Anal. Chem.* **2013**, *85*, 1285−1289.

(33) Pei, J.; Li, Q.; Lee, M. S.; Valaskovic, G. A.; Kennedy, R. T. *Anal. Chem.* **2009**, *81*, 6558−6561.

(34) Kelly, R. T.; Page, J. S.; Marginean, I.; Tang, K.; Smith, R. D. *Angew. Chem., Int. Ed.* **2009**, *48*, 6832−6835.

(35) Samel, B.; Chowdhury, M. K.; Stemme, G. *J. Micromech. Microeng.* **2007**, *17*, 1710−1714.

(36) Basu, A. S. *Lab Chip* **2013**, *13*, 1892−1901.

(37) Ammerman, C. N.; You, S. M. *J. Heat Transfer* **1996**, *118*, 429−435.

(38) Dziewatkoski, M. P.; Daniels, L. B.; Olesik, J. W. *Anal. Chem.* **1996**, *68*, 1101−1109.

(39) Solyom, D. A.; Hieftje, G. M. *J. Am. Soc. Mass Spectrom.* **2003**, *14*, 227−235.

(40) Borovinskaya, O.; Hattendorf, B.; Tanner, M.; Gschwind, S.; Günther, D. *J. Anal. At. Spectrom.* **2013**, *28*, 226−233.

(41) Du, W. B.; Sun, M.; Gu, S. Q.; Zhu, Y.; Fang, Q. *Anal. Chem.* **2010**, *82*, 9941−9947.

(42) Currie, L. A. *Pure Appl. Chem.* **1995**, *67*, 1699−1723.

(43) Olesik, J. W.; Gray, P. J. *J. Anal. At. Spectrom.* **2012**, *27*, 1143−1155.

(44) Ho, K.-S.; Chan, W.-T. *J. Anal. At. Spectrom.* **2010**, *25*, 1114−1122.

(45) Nomizu, T.; Kaneco, S.; Tanaka, T.; Ito, D.; Kawaguchi, H.; Vallee, B. T. *Anal. Chem.* **1994**, *66*, 3000−3004.

(46) Yan, X.; Yang, L.; Wang, Q. *Anal. Bioanal. Chem.* **2013**, *405*, 5663−5670.

(47) Schwarz, G.; Mueller, L.; Beck, S.; Linscheid, M. W. *J. Anal. At. Spectrom.* **2014**, *29*, 221−233.

(48) Bandura, D. R.; Baranov, V. I.; Ornatsky, O. I.; Antonov, A.; Kinach, R.; Lou, X. D.; Pavlov, S.; Vorobiev, S.; Dick, J. E.; Tanner, S. D. *Anal. Chem.* **2009**, *81*, 6813−6822.

(49) Hong, J.; Choi, M.; Edel, J. B.; deMello, A. J. *Lab Chip* **2010**, *10*, 2702−2709.

(50) Lombardi, D.; Dittrich, P. S. *Anal. Bioanal. Chem.* **2011**, *399*, 347−352.

(51) Edgar, J. S.; Milne, G.; Zhao, Y.; Pabbati, C. P.; Lim, D. S.; Chiu, D. T. *Angew. Chem., Int. Ed.* **2009**, *48*, 2719−2722.

(52) Edgar, J. S.; Pabbati, C. P.; Lorenz, R. M.; He, M.; Fiorini, G. S.; Chiu, D. T. *Anal. Chem.* **2006**, *78*, 6948−6954.

(53) Abate, A. R.; Hung, T.; Mary, P.; Agresti, J. J.; Weitz, D. A. *Proc. Natl. Acad. Sci. U.S.A.* **2010**, *107*, 19163−19166.

(54) Bremond, N.; Thiam, A. R.; Bibette, J. *Phys. Rev. Lett.* **2008**, *100*, 024501.

(55) Niu, X.; Gulati, S.; Edel, J. B.; deMello, A. J. *Lab Chip* **2008**, *8*, 1837−1841.

(56) Song, H.; Ismagilov, R. F. *J. Am. Chem. Soc.* **2003**, *125*, 14613−14619.

(57) Song, H.; Chen, D. L.; Ismagilov, R. F. *Angew. Chem., Int. Ed.* **2006**, *45*, 7336−7356.

(58) Baret, J. C.; Miller, O. J.; Taly, V.; Ryckelynck, M.; El-Harrak, A.; Frenz, L.; Rick, C.; Samuels, M. L.; Hutchison, J. B.; Agresti, J. J.; Link, D. R.; Weitz, D. A.; Griffiths, A. D. *Lab Chip* **2009**, *9*, 1850−1858.

(59) Agresti, J. J.; Antipov, E.; Abate, A. R.; Ahn, K.; Rowat, A. C.; Baret, J. C.; Marquez, M.; Klibanov, A. M.; Griffiths, A. D.; Weitz, D. A. *Proc. Natl. Acad. Sci. U.S.A.* **2010**, *107*, 4004−4009.